DOI: 10.7860/JCDR/2025/75736.21147

Original Article

Dentistry Section

An Experimental Study on the Effect of Thermally Oxidised Ti-6Al-4V Substrate on the Surface Characteristics and Composition of Hydroxyapatite Coatings Produced by Modified Cold Gas Spray

NORARNEY AHMAD[1], NOREHAN MOKHTAR[2], SITI NOOR FAZLIAH MOHD NOOR[3], HUSSAIN ZUHAILAWATI[4], SUZIANTI ISKANDAR VIJAYA[5]

ABSTRACT

Introduction: Hydroxyapatite (HA) coatings enhance the bioactivity of Titanium-6% Aluminum-4% Vanadium (Ti-6Al-4VTi-6Al-4V). Conventional plasma spraying often results in amorphous HA phases due to high temperatures. To overcome this, HA coatings can be deposited at lower temperatures using a modified Cold Gas Spray (CGS) technique. The present study compared the effects of thermally oxidised and sand-gritted substrates on the properties of HA coatings.

Aim: To evaluate the impact of thermal oxidation on surface topography, roughness, thickness, phase composition and the Calcium-to-phosphorus (Ca/P) molar ratio of HA coatings applied via modified CGS.

Materials and Methods: An experimental study was conducted at the School of Material and Mineral Resources Engineering, Engineering Campus, Universiti Sains Malaysia (USM), Malaysia, from May 2021 to May 2023. Ti-6Al-4V substrates were sand-gritted and thermally oxidised at temperatures ranging from 450°C to 600°C. HA coatings were applied using the modified CGS. Coatings were analysed using Atomic Force Microscopy (AFM), Backscattered Electron Microscopy (BSEM), X-Ray Diffraction (XRD) and X-ray Fluorescence (XRF) to investigate surface roughness, surface topography, coating thickness and composition. Statistical analysis was performed using the Kruskal-Wallis test for group comparisons, followed by post-hoc Mann-Whitney U tests. A p-value of less than 0.05 was considered statistically significant.

Results: Thermally oxidised substrates exhibited increased surface roughness and microhardness compared to the sand-gritted control. The HA coating on sand-gritted substrates had a roughness of 60.43 nm (IQR=37.41 nm), while oxidised surfaces at 500°C and 600°C resulted in roughness values of 27.61 nm (IQR=51.07 nm) and 33.03 nm (IQR=23.19 nm), respectively. A 2D image showed no aggregation of HA particles. Coating thickness was reduced from 109.0 µm (IQR=45.3 µm) on sand-gritted substrates to 48.4 µm (IQR=12.5 µm) on substrates oxidised at 600°C. The thermally oxidised substrate at 500°C produced a coating thickness of 74.2 µm (IQR=9.40 µm) with a Ca/P ratio of 1.83, meeting the Food and Drug Administration (FDA) standard. XRD confirmed that the phase composition of all coatings was consistent with the original HA powder.

Conclusion: Thermal oxidation of Ti-6Al-4V substrates influences the roughness and thickness of HA coatings' surfaces and the modified CGS technique produces HA coatings suitable for biomedical applications.

Keywords: Bioactive ceramic coatings, Modified deposition techniques, Surface properties, Titanium alloys

INTRODUCTION

Implants have been widely used to repair fractured bones caused by ageing and accidents, with their demand increasing due to longer life expectancy and more active lifestyles [1]. Commercially pure Titanium (Ti) and Titanium alloy (Ti-6Al-4V) are commonly used as biomaterials for dental and orthopaedic implants because of their excellent biocompatibility and mechanical properties [2]. Ti-6Al-4V is considered the gold standard for endosseous dental implants [3], with survival rates ranging from 63.8% to 98% over a period of 10 years [3,4].

Despite their success, Ti-6Al-4V implants can sometimes fail due to issues such as poor osseointegration, aseptic loosening, or late-stage complications linked to patient factors or peri-implantitis [4]. Replacing a failed implant in compromised bone remains challenging, emphasising the need for materials and techniques that enhance implant fixation and osseointegration while minimising biological rejection [3].

Osseointegration, which is the stable connection between bone and metal, depends on surface chemistry and topography [5]. However, as a bioinert material, Ti-6Al-4V exhibits minimal interaction with surrounding tissues [6]. Surface modifications, such as sandblasting followed by acid or alkaline etching, can enhance osseointegration by increasing surface roughness and microporosity [7], although residual blasting material or harmful ion release may negatively impact implant performance.

The HA has been used as a coating material because it is bioactive, thus enhancing biological interactions in the human body following implantation. Furthermore, HA, with a chemical composition of $Ca_{10}(PO_4)_6(OH)_2$, is biocompatible, promoting biological fixation due to its structural similarity to human bone [8,9]. The effect of HA-coated implants has been shown to enhance the stability of implants by promoting early bone ingrowth. Various coating techniques are available to deposit HA onto Ti-6Al-4V to achieve surface properties aimed at optimising their performance in biological environments. Among these techniques are plasma spraying [10], sol-gel coating [11] and CGS coating [12]. While plasma spraying is a common coating technique, its high temperatures often result in undesirable phases that compromise the stability of the coating [12,13]. This can lead

to the formation of other phases such as Tetra-Calcium Phosphate (TTCP) and Calcium Oxide (CaO), which exhibit high dissolution rates in the body's fluids, potentially resulting in implant failure [13]. Therefore, lowering the processing temperature may help suppress the decomposition of HA and the formation of undesirable phases.

Key factors influencing implant performance include phase composition and crystallinity, as well as surface roughness and thickness. Variations in surface topography and roughness significantly affect cellular responses to implants [14]. HA coatings with optimised roughness provide a higher surface area, promoting better interaction with bone and facilitating apatite layer formation [15]. A study has demonstrated that implants with nano-topography encourage greater bone cell proliferation [16]. Therefore, surface roughness is a critical factor affecting osteoblast adhesion and spreading. The ideal HA coating thickness for optimal osteogenesis in biomedical applications is reported to be between 50 and 100 µm [17]. However, the most effective surface topography, roughness and thickness remain uncertain. The findings from the present study may provide valuable insights into enhancing cell adhesion, proliferation and mineralisation.

The oxide layer on the surface of Ti-6Al-4V prevents further oxidation and corrosion by forming a stable titanium oxide passive film, which exhibits high corrosion resistance [18]. This layer reduces metallic ion release, thereby enhancing biocompatibility and improves surface hardness, fatigue resistance, wear resistance and corrosion resistance in simulated body fluids [19]. The anatase and rutile crystal phases demonstrate better bioactivity than the amorphous phase, with anatase promoting cell adhesion and osteogenic activity. Additionally, TiO_2 interlayers serve as barriers to reduce coating cracks and HA decomposition during spraying, thus improving HA crystallinity and promoting calcium and phosphate precipitation for enhanced osteoblastic interaction [13].

The CGS accelerates feedstock powders (5-50 µm) towards a substrate using a convergent-divergent nozzle at low processing temperatures, preserving the original structure and chemical composition of the feedstock materials [20]. This technique is effective for depositing metals, polymers, ceramics and composites. Despite challenges related to the low ductility of ceramics like HA, CGS has successfully produced HA coatings with high crystallinity and minimal phase changes [12,21].

Despite advancements in coating techniques for biomedical implants, achieving homogeneous HA coatings with optimised surface roughness, phase composition and crystallinity on thermally oxidised substrates remains a challenge. To fill this gap in the literature, the present study was conducted to investigate the effects of thermally oxidised Ti-6Al-4V substrates on the surface characteristics and composition of HA coatings produced by modified CGS.

MATERIALS AND METHODS

An experimental study was conducted at the School of Material and Mineral Resources Engineering, Engineering Campus, USM, from May 2021 to May 2023. Ethical approval was not required as the study did not involve human subjects.

Study Procedure

The Ti-6Al-4V substrate was used for coating. Substrates that were not sand-gritted or thermally oxidised were excluded from the study, as were substrates with coating defects or damage, which were excluded from the analysis.

A Ti-6Al-4V plate (Goodfellow, UK) with a thickness of 2 mm was used as the substrate. The commercial powder of HA with the chemical composition $Ca_5(PO_4)_3(OH)$ (purum p.a., ≥90%, Sigma-Aldrich) was utilised in the present study as the feedstock powder. The crystallinity and elemental composition of the powder were verified and additional observations of the powder particles were performed. Silicon Carbide (SiC) paper of various grits was used for grinding the Ti-6Al-4V substrate.

Preparation of substrate material: The purchased Ti-6Al-4V plate was cut into dimensions of 6×6 mm^2. The samples were then processed to achieve three types of surface topography and roughness.

(a) **Smooth substrate:** The smooth surface was prepared for comparison before and after sand-gritting and thermal oxidation treatment. The sample surfaces were polished using 600-grit SiC paper, followed by polishing with 1000-grit SiC paper. Next, the samples were polished with a diamond suspension of 6 µm and an alumina suspension of 0.05 µm to achieve surface uniformity and remove any contamination. The samples were cleaned using distilled water and subjected to ultrasonic cleaning in 99% acetone for 10 minutes. Afterward, the samples were dried and stored in an airtight container containing silica gel.

(b) **Sand-gritted substrate:** For the sand-gritted substrate, the samples were ground using 280-grit SiC paper and ultrasonically cleaned in 99% acetone for 10 minutes.

(c) **Thermally grown titanium oxide layer:** Thermal oxidation was performed to grow the titanium oxide layer. The substrate surfaces were ground using 280-grit SiC paper and ultrasonically cleaned in 99% acetone for 10 minutes prior to thermal oxidation. The thermally oxidised substrates were divided into four groups according to oxidation temperatures of 450°C, 500°C, 550°C and 600°C. Each group was maintained at its respective temperature for one hour, with a heating rate of 10°C/min inside a Carbolite furnace. The substrates were cooled down inside the furnace to room temperature before characterisation.

Characterisation of smooth, sand-gritted and thermally grown titanium oxide layer: The surface topography of the smooth, sand-gritted and thermally oxidised samples at 450°C, 500°C, 550°C and 600°C was evaluated using atomic force microscopy (AFM; Nanonavi SPA 400, SII, Japan). The scan area was set to 5 µm × 5 µm at five different locations in non contact mode at room temperature. The 2D and 3D images, as well as surface roughness (Ra), were obtained and measured using Nanonavi SPIWin software version 5.01C. The data were represented in medians with Interquartile Ranges (IQR).

X-ray diffraction (XRD; Bruker D8 Advance) was used to identify the phase composition of the smooth, sand-gritted and thermally oxidised samples at 450°C, 500°C, 550°C and 600°C. Measurements were conducted in the XRD range of Bragg angles from 10° to 90° using Cu-Kα radiation. The voltage was set to 40 kV with a current of 40 mA. Phase identification was analysed using X'pert HighScore Plus (PANalytical) software version 5.1.

In the present study, the substrate hardness of the smooth, sand-gritted and thermally oxidised samples was evaluated using a LECO Microhardness Tester LM 248AT. Each substrate was dented at nine different locations under a load of 1000 gf, with a dwell time of 15 seconds, using two samples from each group.

(d) **HA coating:** In a conventional CGS method, hot gas steam is used as a feedstock carrier. In the present study, a modified CGS process was developed, as described in a previous study [22], in which the feedstock HA powder was maintained at room temperature. This spraying parameter was chosen to retain the HA properties associated with high temperatures. The summarised modified Cold Spray (CS) parameter values are shown in [Table/Fig-1].

The substrates that were sand-gritted and thermally oxidised were placed inside a CGS chamber and heated to 600°C at an interval of 10°C/min, with a soaking time of one hour. The samples were organised into five groups, each subjected to sand-gritting and thermal oxidation at temperatures of 450°C, 500°C, 550°C and 600°C. The heated samples allowed HA particles to anchor and be deposited on the hard metallic surface. After one hour, the heated

Modified CS spraying parameters	Value	
	Standard conditions	Innovate conditions
Substrate surface preparation	Sand-gritted (280 grit)	Thermally oxidised at different temperature
Chamber temperature and soaking hour	600°C (1 hour)	600°C (1 hour)
Gas utilised	OFN	OFN
Gas temperature	Room temperature	Room temperature
Gas pressure	15 MPa	15 MPa

[Table/Fig-1]: Modified Cold Spray (CS) spraying parameters values.

samples were removed and the HA powder was deposited via Cold Spray on the heated substrates. The samples were sprayed with HA powder ten times to ensure complete coverage. Upon completion, the heated samples were reintroduced into the CGS chamber for cooling before characterisation. The HA deposition on the smooth surface was found to be poor; hence, no deposition was performed on the smooth surface. The surface topography, surface roughness, thickness, coating phase composition and elemental composition of the HA coatings were characterised.

Characterisation of Powder and HA Coatings

The particle size of the powder was measured using a MALVERN Mastersizer 3000 laser-based particle size analyser under wet conditions. The powder's morphology was analysed using a Field Emission Scanning Electron Microscope (FESEM; Zeiss Supra 35VP).

The surface topography and roughness of the HA coating on sand-gritted and thermally oxidised substrates at temperatures of 450°C, 500°C, 550°C and 600°C were evaluated using Atomic Force Microscopy (AFM; Nanonavi SPA 400, SII, Japan). The scan area was set to 5 µm×5 µm at five different locations on two samples from each group in non contact mode at room temperature. The 2D and 3D topographic images and surface roughness (Ra) were obtained and measured using Nanonavi SPIWin software version 5.01C. The data were represented as medians with IQR.

Backscattered Scanning Electron Microscopy (BSEM; Tabletop TEM3000, Hitachi) was used to evaluate the thickness of the HA coating on sand-gritted and thermally oxidised samples at 450°C, 500°C, 550°C and 600°C. The samples were embedded in epoxy resin, then cross-sectioned and sand-gritted using 1000-grit SiC paper, followed by polishing with an alumina suspension of 6 µm. The samples were sputter-coated with a gold-palladium (Au-Pd) mixture and viewed at 300× magnification. The thickness of the coatings was measured three times at five different locations and the thickness was calculated as medians with IQR.

X-ray diffraction (XRD; Bruker D8 Advance) was used to identify the phase composition of the powders and coatings of the HA on sand-gritted and thermally oxidised samples at temperatures of 450°C, 500°C, 550°C and 600°C. The measurements were conducted over a range of Bragg angles from 10° to 90° using Cu-Kα radiation, with the voltage set to 40 kV and the current at 40 mA. Phase identification was analysed using X'pert High Score Plus (PANalytical) software version 5.1.

A semi-quantitative analysis using an X-ray fluorescence (XRF; RIX 3000, PANalytical) spectrometer was performed to measure the elemental composition of the HA powder feedstock and coatings on sand-gritted and thermally oxidised samples at 450°C, 500°C, 550°C and 600°C. The XRF spectrometer was equipped with a rhodium (Rh) X-ray tube, a 4 kW generator and a PC interface with MiniPAL 4 software. The samples were exposed to the X-ray beam, which excited the photons of the elements for elemental analysis. Subsequently, the elemental analysis was used to calculate the Ca/P molar ratio using the following equation [21].

$$\text{nCa or nP} = \frac{M(Ca_{10}(PO_2)6(OH_2))}{M(\text{Ca or P})} \times \%\ \text{wt (Ca or P)}$$

nCa is the weight percent of calcium (nP is for weight percentage of phosphorus), M is the molar mass of HA or P and %wt is corresponds to the weight percentage of Ca or P determined by XRF. The Ca/P ratio is characteristic related to the chemical composition and structural phase of the apatite compound.

STATISTICAL ANALYSIS

The statistical analysis was conducted using Statistical Package for Social Sciences version 26.0. Intergroup comparisons were made using non-parametric Kruskal-Wallis and Mann-Whitney U tests. The median microhardness (HV) was calculated from nine indentations on the surface of each group. The median surface roughness (Ra) was calculated from five scans for each group. Data were analysed for two independent samples. A p-value of less than 0.05 was considered statistically significant.

RESULTS

Surface topography: The surface of the smooth substrate exhibits a uniform topography with smaller grains, as shown in [Table/Fig-2a]. After sand-gritting and undergoing thermal oxidation, topographical changes in the Ti-6Al-4V surfaces can be observed in the images depicted in [Table/Fig-2b-f]. The sand-gritted substrate reveals larger grains along the grooves, resembling pits and valleys. The parallel grooves are a result of the sand-gritting procedure. Following oxidation at 450°C and 500°C, uniform oxide nodule formation is evident. At 600°C, the oxide grains align uniformly along the grooves. The variation in colour reflects differences in signal depth corresponding to peak and valley depths.

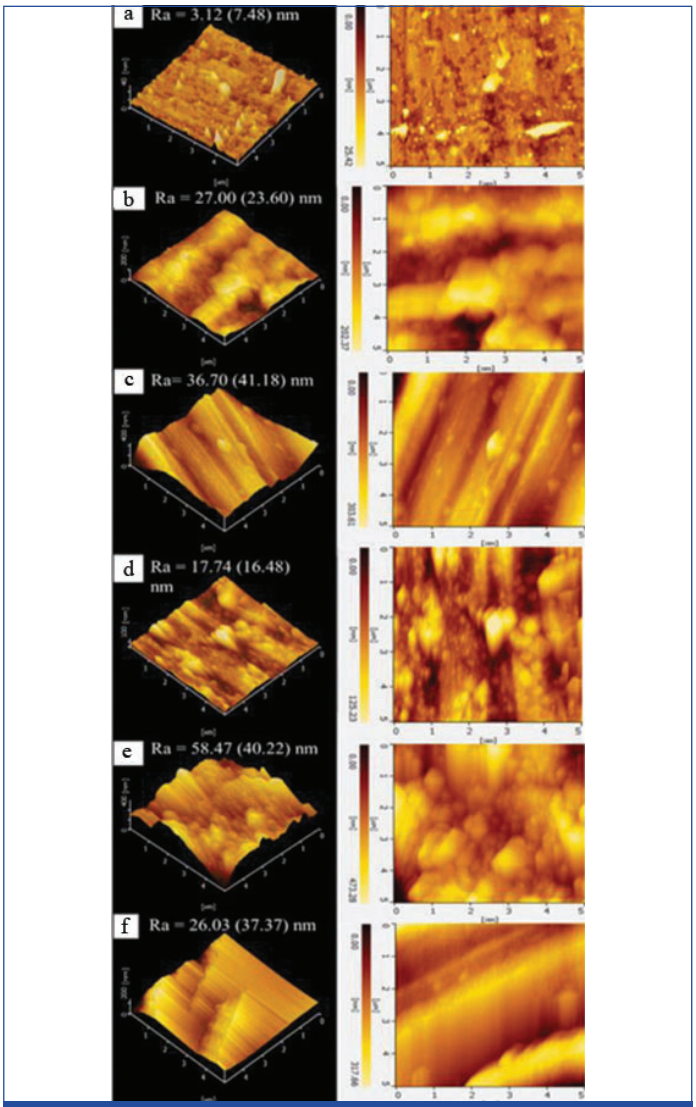

[Table/Fig-2]: The 3D and 2D images of the: a) smooth surface; (b) sand-gritted and thermally oxidation treated at temperatures of; (c) 450°C; (d) 500°C; (e) 550°C; and (f) 600°C.

Surface roughness: The surface roughness (Ra) of the smooth, sand-gritted and thermally oxidised substrates was analysed using AFM, as illustrated in [Table/Fig-3,4]. The smooth Ti-6Al-4V substrate demonstrated a very low surface roughness of 3.12 nm (IQR=7.48 nm), indicating a smooth surface. After sand-grit treatment, the surface roughness increased to 27.00 nm (IQR=23.60 nm). Subsequently, the sand-gritting followed by thermal oxidation resulted in increased surface roughness of the Ti-6Al-4V substrate compared to the untreated (smooth) surface. The analysis revealed that the smooth substrate surface exhibited a statistically significant difference at p=0.004 when compared to the thermally oxidised substrate surfaces, as determined by the Kruskal-Wallis test [Table/Fig-3]. In contrast, the thermal oxidation groups displayed a p-value of 0.065, indicating no statistically significant differences.

Substrate surface n=1	Surface roughnesss, Ra (nm)		Kruskal-Wallis test, p-value
	Medians	Interquartile range	
Smooth	3.12	7.48	0.028**
Sand grit	27.00	23.60	
Smooth	3.12	7.48	0.004**
Sand grit	27.00	23.60	
Thermally oxidised at 450°C	36.70	41.18	
Thermally oxidised at 500°C	17.74	16.48	
Thermally oxidised at 550°C	58.47	40.22	
Thermally oxidised at 600°C	26.03	37.37	
Smooth	3.12	7.48	0.004**
Thermally oxidised at 450°C	36.70	41.18	
Thermally oxidised at 500°C	17.74	16.48	
Thermally oxidised at 550°C	58.47	40.22	
Thermally oxidised at 600°C	26.03	37.37	
Sand grit	27.00	23.60	0.053
Thermally oxidised at 450°C	36.70	41.18	
Thermally oxidised at 500°C	17.74	16.48	
Thermally oxidised at 550°C	58.47	40.22	
Thermally oxidised at 600°C	26.03	37.37	
Thermally oxidised at 450°C	36.70	41.18	0.065*
Thermally oxidised at 500°C	17.74	16.48	
Thermally oxidised at 550°C	58.47	40.22	
Thermally oxidised at 600°C	26.03	37.37	

[Table/Fig-3]: Intergroup comparison of surface roughness (Ra) of smooth, sand-gritted and thermally oxidised surfaces of Ti-6Al-4V substrate.
Kruskal-Wallis test. Statistically significant *p<0.05

Upon subjecting Ti-6Al-4V to thermal oxidation, an observable increase in surface roughness was noted, except at the temperatures of 500°C and 600°C, where the roughness did not significantly differ from that of the sand-gritted substrate. Furthermore, comparisons between the 500°C and 550°C groups, as well as between the 550°C and 600°C groups, demonstrated statistically significant differences with p-values of 0.016 and 0.047 [Table/Fig-4], respectively, highlighting increased oxide formation at elevated temperatures.

Phase Composition

An XRD plot performed on the untreated Ti-6Al-4V and on surfaces that have been thermally oxidised at 450°C, 500°C, 550°C and 600°C, respectively as shown in [Table/Fig-5]. The untreated Ti-6Al-4V exhibited a typical titanium phase structure, specifically the α-Ti structure (Reference code 01-083-4054). Peaks were observed at 2-theta values of 34.92, 38.11, 40.01, 52.90, 63.11, 70.66, 74.48, 76.45, 77.70, 82.30 and 87.18, corresponding to Miller indices (100), (002), (101), (102), (110), (103), (200), (112), (201), (004) and (202). The substrates treated at temperatures ranging

Substrate surface, n=1		Surface roughness, Ra (nm)		Mann-Whitney U test, p-value
		Medians	Interquartile range	
Smooth	Sand grit	27.00	23.60	0.028**
	Thermally oxidised at 450°C	36.70	41.18	0.009**
	Thermally oxidised at 500°C	17.74	16.48	0.016**
	Thermally oxidised at 550°C	58.47	40.22	0.009**
	Thermally oxidised at 600°C	26.03	37.37	0.028**
Sand grit	Thermally oxidised at 450°C	36.70	41.18	0.117
	Thermally oxidised at 500°C	17.74	16.48	0.917
	Thermally oxidised at 550°C	58.47	40.22	0.016**
	Thermally oxidised at 600°C	26.03	37.37	0.754
Thermally oxidised at 450°C	Thermally oxidised at 500°C	17.74	16.48	0.117
	Thermally oxidised at 550°C	58.47	40.22	0.347
	Thermally oxidised at 600°C	26.03	37.37	0.465
Thermally oxidised at 500°C	Thermally oxidised at 550°C	58.47	40.22	0.016**
	Thermally oxidised at 600°C	26.03	37.37	0.602
Thermally oxidised at 550°C	Thermally oxidised at 600°C	26.03	37.37	0.047**

[Table/Fig-4]: Comparison of surface roughness (Ra) of smooth, sand grit and the thermally oxidised surface of Ti-6Al-4V Substrate.
Statistically difference at *p<0.05, Mann-Whitney U test

from 450°C to 600°C also displayed a dominant typical α-Ti phase. It is indicated that a thinner oxide layer was formed due to the penetration of Cu-Kα radiation into the Ti-6Al-4V substrate.

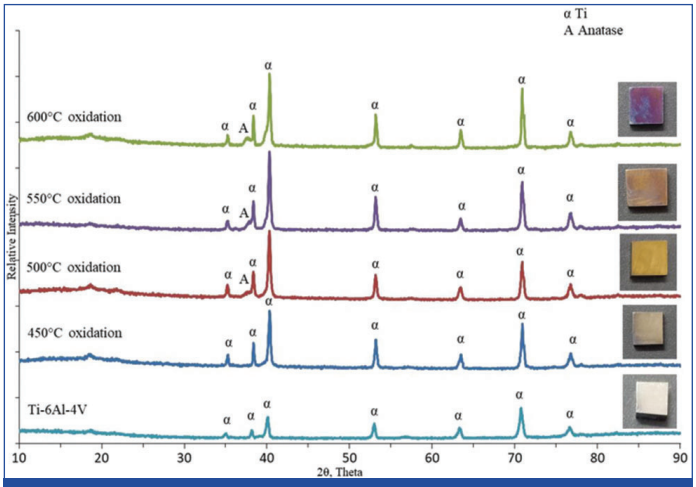

[Table/Fig-5]: The XRD plot of the smooth, Ti-6Al-4V, thermally oxidised Ti-6Al-4V and optical micrography.

During oxidation at 450°C, an amorphous oxide layer was formed, although the peak associated with it was not shown as it exhibited low intensity [22]. As the oxidation temperature increased, the amorphous oxide layer transformed into a crystalline oxide layer. A small peak of anatase (TiO_2, Reference code 04-022-3338) was observed at 500°C, with reflections at the 2θ positions of 38.30, 39.49, 63.59, 77.64 and 85.34, corresponding to (002), (004), (220), (224) and (321).

At 550°C, the thermally oxidised samples exhibited 2θ positions at 25.36, 37.84, 38.29, 38.96, 48.12, 55.87, 63.98, 70.81, 71.35, 76.95, 77.45, 77.91, 84.088 and 85.06, corresponding to (101), (103), (002), (112), (004), (200), (105), (204), (103), (116), (215), (107), (201), (224) and (008). The reflections for the thermally oxidised samples at 600°C were recorded at 25.44, 37.10, 38.30, 38.90, 48.68, 54.12, 55.84, 62.91, 63.36, 63.37, 69.23, 70.87, 74.47, 74.75, 75.93, 76.70, 83.55 and 83.96, corresponding to (101), (103), (002), (112), (200), (105), (211), (213), (204), (110), (116), (103), (107), (200), (215), (112), (303) and (224).

The presence of anatase indicates that a crystalline phase of oxides exists within the oxide layer. Different colours were generated on the thermally oxidised substrates depending on the temperature used in the thermal oxidation process. The optical micrographs of the thermally oxidised substrates exhibited a dominant colour, with small portions displaying different colours across the surfaces. Notably, colours intensified as the oxidation temperature increased from 450°C to 550°C. However, a significant colour change was observed following oxidation at 600°C. The remarkable transition in colour from light yellow to golden brown and purple/blue was indicative of the formation of an oxide layer. It has also been reported that upon oxidation, titanium alloys change colour [23]. Furthermore, the composition of the oxide layer affects the interference of light between the titanium alloy substrate and the oxide layer. Therefore, the colour change depends on the composition of the oxide layer [23].

Microhardness

The median microhardness values along with their IQR is presented in [Table/Fig-6,7]. The untreated surfaces, or smooth substrates, exhibited a microhardness of 314.90 HV (IQR=17.43 HV), whereas the sand-gritted surfaces demonstrated an increased microhardness of 332.80 HV (IQR=13.62 HV). Significant differences in microhardness between untreated substrates and those subjected to thermal oxidation were noted, yielding a p-value of less than 0.01. However, comparisons among the treatments at 500°C and 550°C revealed no significant differences (p-value=0.98), which can be attributed to the consistent crystalline oxide formation, as substantiated by the XRD analysis [Table/Fig-7].

Substrate surface, n=2	Microhardness (HV)		Kruskal-Wallis test, p-value
	Medians	Interquartile Range (IQR)	
Smooth	314.90	17.43	0.024**
Sand grit	332.80	13.62	
Smooth	314.90	17.43	<0.001**
Sand grit	332.80	13.62	
Thermally oxidised at 450°C	329.25	13.75	
Thermally oxidised at 500°C	339.15	26.08	
Thermally oxidised at 550°C	340.90	25.60	
Thermally oxidised at 600°C	346.20	20.07	
Smooth	314.90	17.43	<0.001**
Thermally oxidised at 450°C	329.25	13.75	
Thermally oxidised at 500°C	339.15	26.08	
Thermally oxidised at 550°C	340.90	25.60	
Thermally oxidised at 600°C	346.20	20.07	
Sand grit	332.80	13.62	0.003**
Thermally oxidised at 450°C	329.25	13.75	
Thermally oxidised at 500°C	339.15	26.08	
Thermally oxidised at 550°C	340.90	25.60	
Thermally oxidised at 600°C	346.20	20.07	
Thermally oxidised at 450°C	329.25	13.75	0.004**
Thermally oxidised at 500°C	339.15	26.08	
Thermally oxidised at 550°C	340.90	25.60	
Thermally oxidised at 600°C	346.20	20.07	

[Table/Fig-6]: Comparison of sample hardness of smooth, sand grit and the thermally oxidised surface of Ti-6Al-4V Substrate.
Kruskal Wallis test, Statistical significance at *p<0.05

HA Coating

Feedstock characterisation: The commercially available HA powder exhibits an irregular morphology, as shown in [Table/Fig-8], with a mixture of large and small particles used for coating deposition. The HA powder appears to be composed of very fine agglomerates.

Substrate surface, n=2		Microhardness (HV)		Mann-Whitney U test, p-value
		Medians	Interquartile Range (IQR)	
Smooth	Sand grit	332.80	13.62	<0.001**
	Thermally oxidised at 450°C	329.25	13.75	0.001**
	Thermally oxidised at 500°C	339.15	26.08	<0.001**
	Thermally oxidised at 550°C	340.90	25.60	<0.001**
	Thermally oxidised at 600°C	346.20	20.07	<0.001**
Sand grit	Thermally oxidised at 450°C	329.25	13.75	0.283
	Thermally oxidised at 500°C	339.15	26.08	0.251
	Thermally oxidised at 550°C	340.90	25.60	0.464
	Thermally oxidised at 600°C	346.20	20.07	0.001**
Thermally oxidised at 450°C	Thermally oxidised at 500°C	339.15	26.08	0.074
	Thermally oxidised at 550°C	340.90	25.60	0.134
	Thermally oxidised at 600°C	346.20	20.07	<0.001**
Thermally oxidised at 500°C	Thermally oxidised at 550°C	340.90	25.60	0.988
	Thermally oxidised at 600°C	346.20	20.07	0.031*
Thermally oxidised at 550°C	Thermally oxidised at 600°C	346.20	20.07	0.027**

[Table/Fig-7]: Intergroup comparison of samples hardness of smooth, sand grit and the thermally oxidised surface of Ti-6Al-4V Substrate.
Mann Whitney U-test, Statistically significant at *p<0.05

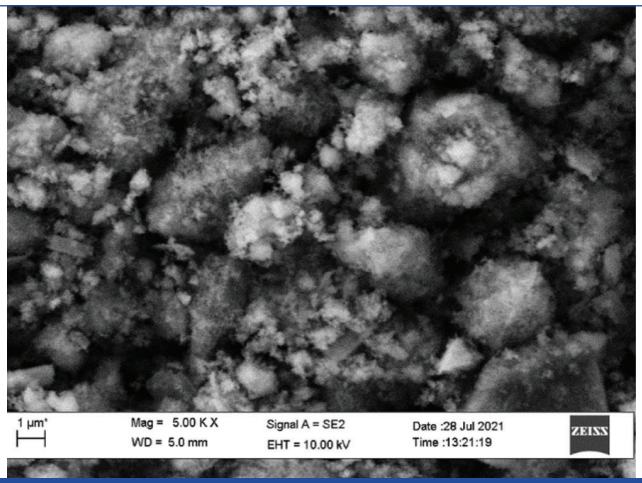

[Table/Fig-8]: The particle of HA powder.

The particle size distribution of the as-received powder is shown in [Table/Fig-9]. As can be observed, the particle distribution indicates a mean diameter (Ømean) of 4.65 µm, with Ø10=1.91 µm and Ø90=13.3 µm. The indexing was performed based on the hexagonal crystal system of space group P63/m. The Ca/P ratio of the powder was found to be 1.68 [Table/Fig-10].

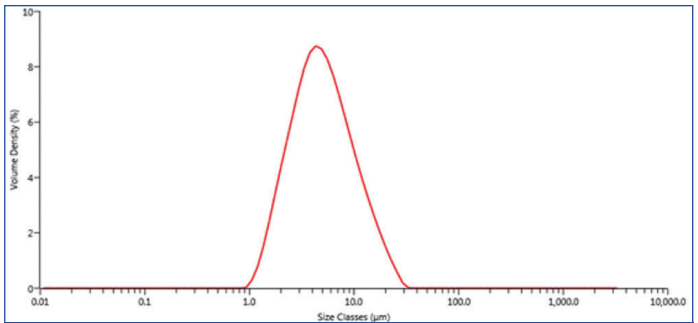

[Table/Fig-9]: The particle size in classes.

Powder	Element (wt%)			Ca/P ratio
	Ca	P	Others (Al, Fe, Cu, Sr, Zr, Pd)	
HA powder	66.68	30.5	2.793	1.68

[Table/Fig-10]: The Cap/P ratio for HA powder feedstock.

Surface topography: The surface topography of the HA coating on the sand-gritted and thermally oxidised substrates at 450°C, 500°C, 550°C and 600°C, respectively as shown in [Table/Fig-11a-e]. The coating exhibited regular compaction of particles due to the hammering effect of HA particles during spraying. The 2D images reveal no aggregation of HA particles; the colour variation indicates the depth and valleys of the coating samples. Moreover, the prepared coating covered the entire Ti-6Al-4V substrate surface.

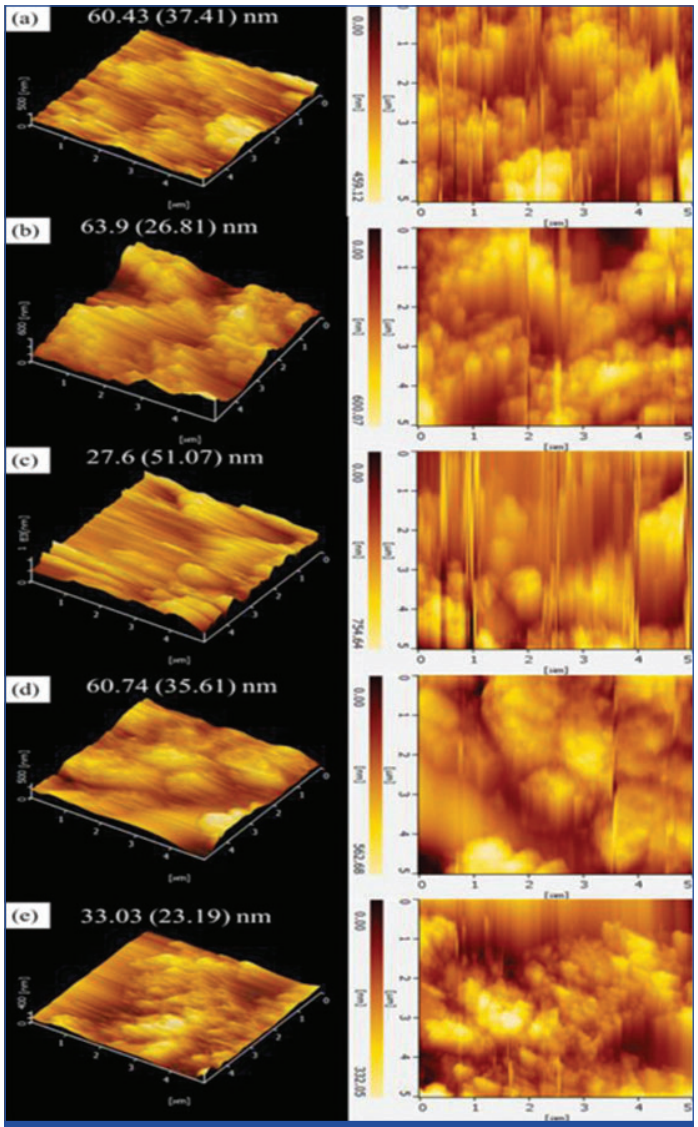

[Table/Fig-11]: The 3D and 2D images of the HA coating on: (a) sand-gritted surface and thermal oxidation-treated substrate surface at: (b) 450°C; (c) 500°C; (d) 550°C; and (e) 600°C.

Surface Roughness

The surface roughness of the HA coating produced by the thermally oxidised surface substrate at 450°C (Ra) was the highest, measuring 63.92 nm (IQR=26.81 nm). In contrast, the HA coating on the thermally oxidised surface at 500°C of Ti-6Al-4V produced lower surface roughness, with a value of 27.61 nm (IQR=51.07 nm). Significant differences in surface roughness were observed among the sand-gritted and thermally oxidised substrate groups, with p-values <0.05 [Table/Fig-12,13].

Coating Thickness

For a better understanding of the HA coating deposition, the thickness of the HA coating on the different thermally oxidised substrates was measured and compared. The spraying parameters remained constant. The HA coating thickness data is presented in [Table/Fig-14,15]. The surface roughening due to sand grit resulted in the highest HA coating thickness. When deposited under the same CS parameters, the HA coating thickness decreased for the thermally oxidised surfaces. The differences in coating thickness among the groups were statistically significant, with a p-value of <0.001 [Table/Fig-14]. However, the HA coating thickness on the sand-gritted surface compared to that treated at 450°C did not show a significant difference, with a p-value of 0.678. The HA coating thickness at 550°C was not significantly different from that at 600°C [Table/Fig-15].

HA coating, n=2	Surface roughness, Ra (nm)		Kruskal wallis test, p-value
	Medians	Interquartile Range (IQR)	
Sand grit	60.43	37.41	0.027**
Thermally oxidised at 450°C	63.92	26.81	
Thermally oxidised at 500°C	27.61	51.07	
Thermally oxidised at 550°C	60.74	35.61	
Thermally oxidised at 600°C	33.03	23.19	
Thermally oxidised at 450°C	63.92	26.81	0.037**
Thermally oxidised at 500°C	27.61	51.07	
Thermally oxidised at 550°C	60.74	35.61	
Thermally oxidised at 600°C	33.03	23.19	

[Table/Fig-12]: HA coating surface roughness.
Ra=surface roughness (nm). The non-normality assumption is fulfilled. **statistically different at p<0.05, Kruskal-Wallis test

HA coating, n=2		Surface roughness, Ra (nm)		Mann-Whitney U Test, p-value
		Median	Interquartile Range (IQR)	
Sand grit	Thermally oxidised at 450°C	63.92	26.81	0.965
	Thermally oxidised at 500°C	27.61	51.07	0.094
	Thermally oxidised at 550°C	60.74	35.61	0.546
	Thermally oxidised at 600°C	33.03	23.19	0.008**
Thermally oxidised at 450°C	Thermally oxidised at 500°C	27.61	51.07	0.102
	Thermally oxidised at 550°C	60.74	35.61	0.453
	Thermally oxidised at 600°C	33.03	23.19	0.007**
Thermally oxidised at 500°C	Thermally oxidised at 550°C	60.74	35.61	0.102
	Thermally oxidised at 600°C	33.03	23.19	0.757
Thermally oxidised at 550°C	Thermally oxidised at 600°C	33.03	23.19	0.047**

[Table/Fig-13]: Comparison test for HA coating surface roughness.
Ra=surface roughness (nm). **statistically different at p<0.05, *the Mann-Whitney test

HA coating, n=1	Coating thickness (µm)		Kruskal-Wallis test, p-value
	Median	Interquartile Range (IQR)	
Sand grit	109.0	45.3	<0.001***
Thermally oxidised at 450°C	105.0	25.4	
Thermally oxidised at 500°C	74.2	9.4	
Thermally oxidised at 550°C	44.6	22.7	
Thermally oxidised at 600°C	48.4	12.5	
Thermally oxidised at 450°C	105.0	25.4	<0.001***
Thermally oxidised at 500°C	74.2	9.4	
Thermally oxidised at 550°C	44.6	22.7	
Thermally oxidised at 600°C	48.4	12.5	

[Table/Fig-14]: A comparative analysis of HA coating thickness.
Kruskal Wallis test, p-value <0.05

HA coating, n=1		Coating thickness (μm)		Mann-Whitney U test, p-value
		Median	Interquartile Range (IQR)	
Sand grit	Thermally oxidised at 450°C	105.0	25.4	0.678
	Thermally oxidised at 500°C	74.2	9.4	<0.001***
	Thermally oxidised at 550°C	44.6	22.7	<0.001***
	Thermally oxidised at 600°C	48.4	12.5	<0.001***
Thermally oxidised at 450°C	Thermally oxidised at 500°C	74.2	9.4	<0.001***
	Thermally oxidised at 550°C	44.6	22.7	<0.001***
	Thermally oxidised at 600°C	48.4	12.5	<0.001***
Thermally oxidised at 500°C	Thermally oxidised at 550°C	44.6	22.7	<0.001***
	Thermally oxidised at 600°C	48.4	12.5	<0.001***
Thermally oxidised at 550°C	Thermally oxidised at 600°C	48.4	12.5	0.648

[Table/Fig-15]: Intergroup comparison of HA coating thickness.
Mann-Whitney U test, p-value <0.05, significant

The BSEM cross-section images of the HA coatings, revealing the HA layer at low magnification as shown in [Table/Fig-16a-e]. The HA coatings and the substrate were clearly differentiated; the light region corresponds to the substrate, while the grey region represents the HA layer. The HA coatings were dense, with no observable pores and no delamination was found on the surface of the Ti-6Al-4V substrate.

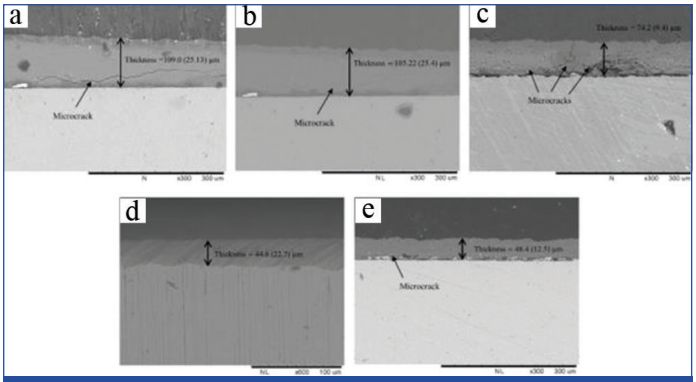

[Table/Fig-16]: Cross-sectional of the HA coating at low magnification on the: (a) sand-gritted surface and thermal oxidation-treated at; (b) 450°C; (c) 500°C; (d) 550°C; and (e) 600°C with measured coating thickness labelled in the images.

Coating Phase Composition

The XRD analysis of HA coatings on both sand-gritted and thermally oxidised Ti-6Al-4V surfaces is presented in [Table/Fig-17] and compared against the feedstock powder pattern. The α-Ti peak was observed, indicating the penetration of Cu-Kα radiation into the Ti-6Al-4V substrate. The diffraction pattern of the as-received feedstock powder can be assigned to a pure HA phase (space group P3/m), which aligns well with reference code 04-007-2837 at the diffraction angle 2θ. As expected, the XRD patterns of the HA coatings reveal that HA is still maintained as the major phase. It can be observed that the most intense diffraction peaks of HA have narrowed significantly, indicating a high crystallinity of the HA.

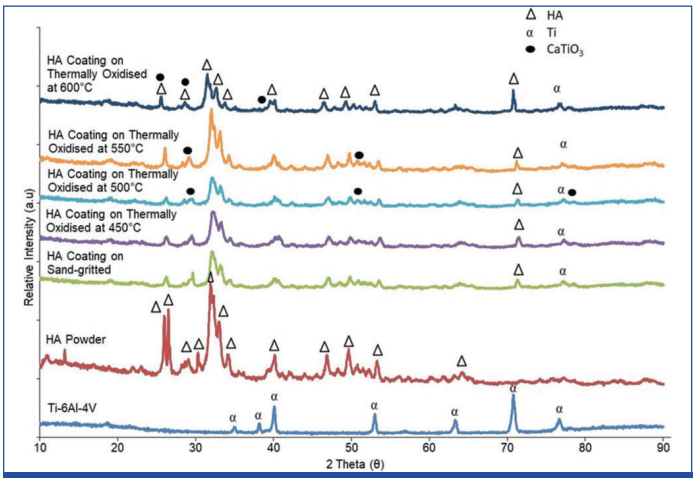

[Table/Fig-17]: The XRD plot acquired from HA coating using modified Cold Gas Spray (CGS) and from the as-received HA powder and the polished surface of Ti-6Al-4V.

Additionally, $CaTiO_3$ was also present in the as-sprayed coatings. No β phases were detected in the XRD spectra of the substrate due to the heating of the substrate during deposition. The HA coating on the sand-gritted surface, indexed with reference code 04-023-4123, shows a peak of 2θ reflection at 26.165, corresponding to (200) when compared to the reference data. The XRD pattern of the HA coating on the thermally oxidised surface at 450°C (reference code 04-010-6314) presents 2θ positions at 31.60, 32.01, 32.75 and 40.21, which correspond to (121), (112), (030) and (101) and are indexed to the HA phase.

The HA coating on the thermally oxidised surface at 500°C, with reference code 01-086-0740, shows reflections at 2θ positions 23.13, 26.13, 28.38, 29.20, 32.04, 32.45, 33.17, 34.32, 49.73, 50.74 and 53.43, corresponding to (020), (002), (012), (120), (121), (112), (030), (022), (123), (231) and (004). The reference code 04-010-7763 is indexed as CaTiO3 at 2θ positions 32.45 and 51.53, corresponding to (112) and (140).

The HA coating on the thermally oxidised surface at 550°C, indexed to HA with reference code 04-023-4123, shows peaks at 2θ positions 26.03, 29.03, 29.08, 29.17, 31.81, 31.83, 31.88, 31.92, 31.97, 31.99, 32.01, 33.00, 33.05, 33.16 and 53.34, corresponding to (200), (031), (023), (012), (132), (131), (123), (-131), (-123), (121), (-112), (112), (033), (030), (003) and (400). The reference code 04-025-6588 is indexed to $CaTiO_3$ at 2θ positions 32.36, 32.38, 32.39 and 32.41, corresponding to (-211), (-221), (211) and (-212), respectively.

The HA coating on the thermally oxidised surface at 600°C, indexed to HA with reference code 01-080-7128, shows 2θ positions at 31.84, 32.56, 33.71, 46.37, 49.16 and 52.88, corresponding to (112), (030), (022), (222), (213) and (004). Additionally, peaks of CaTiO3 (reference code 04-007-9435) and HA may overlap, contributing to the high intensity of the reflections at 2θ positions 25.51, 28.58, 31.42 and 39.47, corresponding to (002), (120), (121) and (310). Moreover, broadening and weak intensity of HA, which are indicative of poor crystallinity and/or the crystallite size of HA being in the submicron to nanoscale, can be observed in all coatings. However, no other HA phases, such as CaO, tricalcium phosphate, or TTCP, which are usually present in the thermal spray of HA coatings, were found. This confirms that the modified CGS process is capable of maintaining the HA phase during coating application and can avoid phase decomposition.

Coating Elemental Composition

The measurement of Ca, P and O content in the coating using XRF, illustrating the evolution of the chemical composition during coating formation is presented in [Table/Fig-18]. All samples exhibited significant levels of Ca and P, indicating effective deposition of HA onto the surface. Ti was detected due to X-ray penetration and the thickness of the HA coating. Based on the results, the percentage of Ca increased after thermal oxidation, except for the substrate treated by thermal oxidation at 600°C (HA coating on thermally oxidised at 600°C).

The elemental composition of Ca and P affected the value of the Ca/P molar ratio, which ideally should be 1.67 for stoichiometric HA. However, stable HA phases exist over a range of 1.3 to 1.8. Therefore, the modified CGS process was able to produce a stable coating, except for the HA coating on the thermally oxidised substrate at 450°C. Furthermore, the Ca/P molar ratio of the HA coating on the thermally oxidised substrate at 500°C was in the range of 1.67 to 2.08, which meets the required Ca/P molar ratio for coatings as outlined in FDA procedures following International Organisation for Standardisation (ISO) standards [21].

HA coating, n=1	Element (wt%)						Ca/P ratio
	Ca	P	Ti	Al	V	Others (Fe, Cu, Zn, Re, Pt)	
Sand grit	21.27	21.0	50.87	3.7	3.00	0.2311	1.56
Thermally oxidised at 450°C	23.39	17.3	48.20	8.5	2.31	0.2438	2.08
Thermally oxidised at 500°C	28.79	24.3	40.75	3.2	2.71	0.1796	1.83
Thermally oxidised at 550°C	30.68	24.6	38.64	3.2	2.56	0.3098	1.52
Thermally oxidised at 600°C	15.73	18.6	57.89	4.6	2.95	0.2374	1.31

[Table/Fig-18]: The elemental analysis of as-deposited HA coatings measured by XRF.

DISCUSSION

The surface of an implant is crucial for successful osseointegration and influences the behaviour of osteoblast cells. Coating with HA improves surface properties, leading to better implant and hard tissue responses for early osseointegration and fixation [24]. Therefore, the modified CGS process was explored to produce HA coatings. As the modified CGS is still in its development phase, it is essential to investigate various operational parameters to enhance and optimise the process for fabricating HA coatings. The characteristics of the interlayer titanium oxide were particularly important in determining the properties of the HA coating.

Consequently, the properties of the thermally grown titanium oxide were also investigated. The HA coating surface was then analysed in terms of topography, roughness, thickness and composition.

Thermally Oxidised Substrate

When Ti-6Al-4V is heated in air, oxide layers are formed through the reaction of the substrate with the surrounding air, depending on the temperature range. Titanium can react with N_2, H_2 and O_2, while Aluminium (Al) and Vanadium (V) also react with O_2 [14]. Consequently, the oxide layer produced may contain Ti and O and/or other elements such as Al and V. XRD analyses have confirmed that the oxide layer was formed. The different colours of the oxide are attributed to colour interference and the non uniform oxidation of the differently orientated α phase [25].

In this experiment, grinding and polishing were employed prior to thermal oxidation to alter the surface roughness of the substrate. The sand-gritted surface exhibited uniform parallel grooves due to the grinding process. It has been demonstrated that grinding modified the surface roughness of the Ti-6Al-4V. Results indicate that the smoothest surface had the lowest roughness, achieved through the polishing steps that transitioned from high-grit SiC paper to fine-particle media suspension. It was observed that the polished metal substrate had a uniform pattern and roughness on the surface [15].

The surface roughness of the thermally oxidised surfaces increased due to the inhomogeneity and irregularity of oxide formation, characterised by large oxide nodules, as observed [16]. Furthermore, the oxide formed along the parallel grinding grooves. Upon heating, the formation of large oxide nodules increased surface roughness at oxidation temperatures of 450°C and 550°C. Additionally, an increase in temperature led to irregular surface roughness at 550°C due to greater oxide nodule formation. AFM images showed that parallel grooves remained on the surface throughout the thermal oxidation process. Lower surface roughness, relatively smooth, occurred after thermal oxidation at 500°C and 600°C. A comparison of these surface topographies reveals smaller oxide nodules dispersed throughout the surface. Observations by [17] also found lower surface roughness at 600°C. Furthermore, the oxide layer formed enhances coating properties and aids in HA deposition during spraying.

Thermal oxidation also induced hardness differences between sand-gritted and smooth substrates. The increase in hardness value for the oxidised samples is primarily due to the formation of an oxide phase such as anatase, which has a hardness of approximately 815 HV [16,19] within the microstructure. Another study supports the notion that thermal oxidation increases the hardness of Ti-6Al-4V [26]. Additionally, all thermally oxidised substrates indicating anatase formation showed a significant increase in microhardness. The increase in hardness is important to prevent surface wear of the implants in biomedical applications [27]. Thus, more detailed studies on HA deposition are needed.

The CS method involves using low operational temperatures to spray feedstock particles without melting them and without causing heat damage to the substrate during deposition. Moreover, CS is likely the most straightforward and cost-effective deposition approach, as it is regulated by only a handful of parameters. Although the deposition of ceramics by modified CGS has not been extensively investigated, other deposition techniques such as vacuum CS [20] and spray pyrolysis/Aerosol Deposition (AD) [28] have reported similar approaches.

In the current experiment, HA particles collide with and deposit on sand-gritted and thermally oxidised substrates with hardness values between 332.8 HV and 346.20 HV. AFM images show crater formation in the HA coating, yet the overall surface roughness is reduced. The decrease in HA thickness on harder substrates indicates that substrate hardness significantly affects deposition. The reduced thickness and lower roughness may be attributed to the nodule oxide filling in the craters. Substrate roughness and hardness impact these results.

For a surface where the substrate roughness is finer than the particle size, the particles are unable to reach and adhere well to the valleys between the surface asperities. Conversely, if the surface roughness is much coarser than the particle size, the contact area becomes insufficient, resulting in an effect similar to spraying particles onto a flat surface [27]. This interaction between surface roughness and particle size further elucidates the observed reduction in HA coating thickness and roughness on harder substrates.

The HA coatings fabricated by modified CGS exhibit a dense microstructure, akin to ceramic coatings on magnesium substrates [12,29]. Particle size plays a significant role in the characteristics of the coating due to the solid-state nature of the cold spray deposition process. The submicron particle size contributes to a dense microstructure. Other deposition techniques, such as AD, have also reported a dense microstructure [28]. Furthermore, smaller particles are more easily accelerated due to their lower inertia [29], which is particularly notable in high-pressure CS methods [26]. The use of fine particles is advantageous in CGS, as the impact energy may be directly utilised for compaction [30].

The modified CS method produced coatings with lower roughness compared to Atmospheric Plasma Spray (APS) coatings, High-Velocity Oxy-Fuel (HVOF) coatings and conventional CS methods. Notably, HA coatings on sand-gritted and thermally oxidised surfaces at specific temperatures resulted in higher roughness due to substrate characteristics [27]. Moreover, HA coatings on thermally oxidised surfaces at 600°C showed comparable roughness values within a suitable range of 30-50 nm for hMSC cell adhesion. These observations underscore the influence of deposition technique and substrate roughness on coating properties.

Among the coatings, the sand-gritted surfaces were preferred for achieving thicker coatings compared to thermally oxidised surfaces. It is believed that substrate roughness is a crucial factor in facilitating the thick deposition of HA. Previous researchers [12], using a similar

modified CGS method, also achieved high coating thickness on rough magnesium substrates, confirming the importance of surface preparation. Notably, the number of sprays has minimal impact on coating thickness and was not a variable in this study. Therefore, roughening the substrate before deposition is recommended to facilitate coating build-up and achieve thicker coatings. Although the thickness of HA coating is not established by the manufacturer, a commercial range of 50-75 µm is typically required [21,31]. Hence, the HA coating on the thermally oxidised surface at 500°C provided a coating thickness of 74.2 µm (IQR=9.4 µm), which closely aligns with these commercial standards compared to the HA coating on the sand-gritted surface. Furthermore, an ideal thickness of 40 to 50 µm has been suggested to promote cell adhesion and the proliferation of cells responsible for bone formation [32]. Thus, the HA coating on the thermally oxidised surface at 550°C and 600°C provides an ideal coating thickness.

Although the HA coating layer was successfully deposited, some microcracks exist within the coating layer. In contrast, microcracks were not observed in the HA coatings on the thermally grown titanium oxides, except for the HA coating on a thermally oxidised surface at 500°C. The microcracks in the HA coating layer could primarily be attributed to the thermal mismatch between the Ti-6Al-4V substrate and the HA coating, or occurring during the cooling process. The thermally oxidised layer could alleviate the Coefficient of Thermal Expansion (CTE) mismatch between the HA coating and the substrate prior to HA deposition. Additionally, the heated Ti-6Al-4V would reduce the CTE value [33].

Considering equivalent spraying conditions, the differences between coatings primarily relate to thickness and roughness due to substrate characteristics. Plasma spraying often exhibits secondary phases [18]. While conventional CGS heats the gas for feedstock powder deposition, modified CGS injects the feedstock powder at room temperature. The benefit of this process is that it allows the coating to be deposited without exposing the feedstock powders to high temperatures that could cause phase changes. Thus, modified CGS offers an advantage with the room temperature processing of feedstock powders, resulting in no phase changes in the coatings compared to the original feedstock [34]. In the current experiment, both the HA particles and the gas temperature were maintained at room temperature. The CS process preserves the original phase of HA powder, even when deposited on a hot substrate. No Tetracalcium Phosphate (TTCP) or Calcium Oxide (CaO) was detected in the HA coatings, as these low-temperature processes prevent HA particles from melting. However, a peak of Calcium Titanate ($CaTiO_3$) was observed due to hydroxyl accumulation during coating build-up. The anatase phase in thermally oxidised titanium substrates facilitates the decomposition of HA, forming $CaTiO_3$. This reaction, confirmed in various studies [31,33], is beneficial for osteoblast adhesion, making thermally oxidised substrates with anatase advantageous for reducing HA decomposition and enhancing bioactivity.

The cross-section of the HA coating deposited on Ti-6Al-4V reveals a thick layer, indicating coating build-up and a higher deposition rate. The feedstock powder consists of fine particles with a closely agglomerated morphology. These irregularly shaped agglomerate particles were deposited on the ceramic. The prepared coatings demonstrate continuous coverage, with a notably thicker and more defined coating on the sand-gritted substrate compared to the thermally oxidised substrate. Detailed observations also show no delamination, as most of the impact particles adhere well to each other, contributing to the build-up. Although ceramic particles cannot deform under spray particle impacts, the tamping effect compacts particles under high impact pressure [35], resulting in a dense coating with successive particle deposition.

Under the same spraying conditions, no large pores are visible due to the continuous impact of particles, which prevents the formation of significant voids. The agglomeration of feedstock enhances its flowability [26,35], allowing it to be transported by N_2 gas to the substrate more effectively. Despite these similarities, the thickness of the coating differs between the sand-gritted and thermally oxidised substrates. The sand-gritted surface resulted in a thicker coating than the thermally oxidised substrate. Given that the deposition parameters are consistent for both types of coatings, it appears that substrate roughness is responsible for this difference.

Limitation(s)

Despite the valuable findings, the present study has some limitations. First, the analysis was conducted on a limited number of substrates, which may not fully represent the variety of surface treatments available. Second, the study focused solely on short-term performance and long-term degradation and wear were not assessed. Finally, the use of only Ti-6Al-4V substrates limits the generalisability of the results to other materials commonly used in biomedical applications.

CONCLUSION(S)

The present study demonstrated the potential of modified CGS to fabricate HA coatings on thermally oxidised Ti-6Al-4V substrates. The results revealed that thermal oxidation influenced substrate properties, affecting HA coating topography, roughness and thickness. Substrates treated at 500°C provided an optimal balance, achieving an ideal coating thickness and a Calcium-to-phosphorus (Ca/P) molar ratio that aligns with implant requirements. Increasing the thermal oxidation temperature enhanced surface roughness, promoting bone cell adhesion and proliferation. Sand-gritted surfaces yielded the highest coating thickness, while all coatings exhibited high crystallinity with no phase changes, supporting osteoblast differentiation. These findings highlight the promise of modified CGS for tailoring coating properties to improve implant biocompatibility.

Authors' contribution: NA: Conceptualisation, methodology, investigation, writing - original draft; NM: Conceptualisation, methodology and supervision, writing - review and editing; SNFMN: Supervision, writing - review and editing; SIV: Writing - review and editing; HZ: Methodology, supervision, writing - review and editing.

Acknowledgement

The authors would like to thank the Department of Dental Science, Advanced Medical and Dental Institute (AMDI) Universiti Sains Malaysia (USM) and Biomaterials Niche Group, School of Materials and Mineral Resources Engineering, Universiti Sains Malaysia (USM) for providing the equipment in conducting this study.

REFERENCES

[1] Gautam S, Bhatnagar D, Bansal D, Batra H, Goyal N. Biomedical Engineering advances recent advancements in nanomaterials for biomedical implants. Biomed Eng Adv [Internet]. 2022;3:100029. Available from: https://doi.org/10.1016/j.bea.2022.100029.

[2] Kaur M, Singh K. Review on titanium and titanium based alloys as biomaterials for orthopaedic applications. Mater Sci Eng C Mater Biol Appl [Internet]. 2019;102:844-62. Available from: https://doi.org/10.1016/j.msec.2019.04.064.

[3] Howe MS, Keys W, Richards D. Long-term (10-year) dental implant survival: A systematic review and sensitivity meta-analysis. J Dent [Internet]. 2019;84:09-21. Available from: https://doi.org/10.1016/j.jdent.2019.03.008.

[4] Buser D, Janner SF, Wittneben JG, Brägger U, Ramseier CA, Salvi GE. 10-year survival and success rates of 511 titanium implants with a sandblasted and acid-etched surface: A retrospective study in 303 partially edentulous patients. Clin Implant Dent Relat Res. 2012;14(6):839-51. Doi: 10.1111/j.1708-8208.2012.00456.x. PMID: 22897683.

[5] Albrektsson T, Wennerberg. On osseointegration in relation to implant surfaces. Clin Implant Dent Relat Res. 2019;21 Suppl 1:04-07.

[6] Liu W, Zhang G, Wu J, Zhang Y, Liu J, Luo H, et al. Insights into the angiogenic effects of nanomaterials: Mechanisms involved and potential applications. J Nanobiotechnology [Internet]. 2020;18(1):01-22. Available from: https://doi.org/10.1186/s12951-019-0570-3.

[7] Scarano A, Piattelli A, Quaranta A, Lorusso F. Bone response to two dental implants with different sandblasted/acid-etched implant surfaces: A histological and histomorphometrical study in rabbits. Biomed Res Int. 2017:2017:8724951.

[8] Chen X, Ji G, Bai X, Yao H, Chen Q, Zou Y. Microstructures and properties of cold spray nanostructured HA coatings. J Therm Spray Technol [Internet]. 2018;27(8):1344-55. Available from: https://doi.org/10.1007/s11666-018-0776-1.

[9] Winnicki M. Advanced functional metal-ceramic and ceramic coatings. Coatings. 2021;11(i):1044.
[10] Ke D, Vu AA, Bandyopadhyay A, Bose S. Compositionally graded doped hydroxyapatite coating on titanium using laser and plasma spray deposition for bone implants. Acta Biomater [Internet]. 2019;84:414-23. Available from: https://doi.org/10.1016/j.actbio.2018.11.041.
[11] Ayu HM, Izman S, Daud R, Krishnamurithy G, Shah A, Tomadi SH, et al. Surface modification on CoCrMo alloy to improve the adhesion strength of hydroxyapatite coating. Procedia Eng [Internet]. 2017;184:399-408. Available from: http://dx.doi.org/10.1016/j.proeng.2017.04.110.
[12] Hasniyati M, Zuhailawati H, Sivakumar R, Dhindaw BK, Noor SNFM. Cold spray deposition of hydroxyapatite powder onto magnesium substrates for biomaterial applications. Surf Eng. 2015;31(11):867-74.
[13] Bose S, Ke D, Vu AA, Bandyopadhyay A, Goodman SB. Thermal oxide layer enhances crystallinity and mechanical properties for plasma-sprayed hydroxyapatite biomedical coatings. ACS Appl Mater Interfaces. 2020;12(30):33465-72.
[14] Ma K, Zhang R, Sun J, Liu C. Oxidation mechanism of biomedical titanium alloy surface and experiment. Int J Corros. 2020;2020:1678615.
[15] Jongprateep O, Inseemeesak B, Techapiesancharoenkij R, Bansiddhi A, Vijarnsorn M. Effects of surface modification processes on the adhesion of hydroxyapatite layers coated onto titanium substrates. J Met Mater Miner. 2019;29(4):69-79.
[16] Aniołek K, Kupka M. Mechanical, tribological and adhesive properties of oxide layers obtained on the surface of the Ti-6Al-7Nb alloy in the thermal oxidation process. Wear [Internet]. 2019;432-33:202929. Available from: https://doi.org/10.1016/j.wear.2019.202929
[17] Blum M, Sayed M, Mahmoud EM, Killinger A, Gadow R, Naga SM. In vitro evaluation of biologically derived hydroxyapatite coatings manufactured by high velocity suspension spraying. J Therm Spray Tech. 2021;30:1891-904. Available from: https://doi.org/10.1007/s11666-021-01265-0.
[18] Vahabzadeh S, Roy M, Bandyopadhyay A, Bose S. Phase stability and biological property evaluation of plasma sprayed hydroxyapatite coatings for orthopedic and dental applications. Acta Biomater [Internet]. 2015;17:47-55. Available from: http://dx.doi.org/10.1016/j.actbio.2015.01.022.
[19] Wang G, Li J, Lv K, Zhang W, Ding X, Yang G, et al. Surface thermal oxidation on titanium implants to enhance osteogenic activity and in vivo osseointegration. Sci Rep. 2016;6:01-13.
[20] Moridi A, Hassani-Gangaraj SM, Guagliano M, Dao M. Cold spray coating: Review of material systems and future perspectives. Surf Eng. 2014;30(6):369-95.
[21] Quirama A, Echavarría AM, Meza JM, Osorio J, Bejarano GG. Improvement of the mechanical behavior of the calcium phosphate coatings deposited onto Ti_6Al_4V alloy using an intermediate TiN/TiO_2 bilayer. Vacuum [Internet]. 2017;146:22-30. Available from: https://doi.org/10.1016/j.vacuum.2017.09.024.
[22] Vilardell AM, Cinca N, Dosta S, Cano IG, Guilemany JM. Feasibility of using low pressure cold gas spray for the spraying of thick ceramic hydroxyapatite coatings. International Journal of Applied Ceramic Technology. 2018;16:01-09. Doi: 10.1111/ijac.13088.
[23] Peng W, Zeng W, Zhang Y, Shi C, Quan B, Wu J. The effect of colored titanium oxides on the color change on the surface of Ti-5Al-5Mo-5V-1Cr-1Fe alloy. J Mater Eng Perform. 2013;22(9):2588-93.
[24] Harun WSW, Asri RIM, Alias J, Zulki FH, Kadirgama K, Ghani SAC, et al. A comprehensive review of hydroxyapatite-based coatings adhesion on metallic biomaterials. Ceramics International. 2018;44(2):1250-68.
[25] Sasikumar Y, Indira K, Rajendran N. Surface modification methods for titanium and its alloys and their corrosion behavior in biological environment: A review. J Bio Tribo Corros. [Internet]. 2019;36:5. Available from: http://dx.doi.org/10.1007/s40735-019-0229-5.
[26] García-Rueda AK, Guzmán-Castillo D, García-González L, Zamora-Peredo L, Hernández-Torres J. Surface modification of a Ti6Al4V alloy by thermal oxidation to improve its tribological properties. Materials Letters. 2022;317:132082. Doi: 10.1016/j.matlet.2022.132082.
[27] Liao TY, Biesiekierski A, Berndt CC, King PC, Ivanova EP, Thissen H, et al. Multifunctional cold spray coatings for biological and biomedical applications: A review. Prog Surf Sci [Internet]. 2022;97(2):100654. Available from: https://doi.org/10.1016/j.progsurf.2022.100654.
[28] Hahn B, Hahn BD, Park DS, Park DS, Choi J, Choi JJ, et al. Dense nanostructured hydroxyapatite coating on titanium by aerosol deposition. J Am Ceram Soc. 2009;92(3):683-87.
[29] Noorakma ACW, Zuhailawati H, Aishvarya V, Dhindaw BK. Hydroxyapatite-coated magnesium-based biodegradable alloy: Cold spray deposition and simulated body fluid studies. J Mater Eng Perform. 2013;22(10):2997-3004.
[30] Prisco U. Size-dependent distributions of particle velocity and temperature at impact in the cold-gas dynamic-spray process. J Mater Process Technol [Internet]. 2015;216:302-14. Available from: http://dx.doi.org/10.1016/j.jmatprotec.2014.09.013.
[31] Neto JVC, Teixeira ABV, Cândido dos Reis A. Hydroxyapatite coatings versus osseointegration in dental implants: A systematic review. J Prosthet Dent [Internet]. 2023:S0022-3913(23)00631-5. Available from: https://doi.org/10.1016/j.prosdent.2023.09.019.
[32] Ivanov S, Gushchina M, Artinov A, Khomutov M, Zemlyakov E. Effect of elevated temperatures on the mechanical properties of a direct laser deposited ti-6al-4v. Materials (Basel). 2021;14(21):6432.
[33] Webster TJ, Ergun C, Doremus RH, Lanford WA. Increased osteoblast adhesion on titanium-coated hydroxylapatite that forms $CaTiO_3$. J Biomed Mater Res- Part A. 2003;67(3):975-80.
[34] Sun W, Chu X, Lan H, Huang R, Huang J, Xie Y, et al. Current implementation status of cold spray technology: A short review. J Therm Spray Technol [Internet]. 2022;31(4):848-65. Available from: https://doi.org/10.1007/s11666-022-01382-4.
[35] Chen QY, Zou YL, Chen X, Bai XB, Ji GC, Yao HL, et al. Morphological, structural and mechanical characterization of cold sprayed hydroxyapatite coating. Surf Coatings Technol [Internet]. 2019;357(October 2018):910-23. Available from: https://doi.org/10.1016/j.surfcoat.2018.10.056.

PARTICULARS OF CONTRIBUTORS:
1. Student, Department of Dental Sciences, Advanced Medical and Dental Institute, Universiti Sains Malaysia, Pulau Pinang, Malaysia.
2. Associate Professor, Department of Dental Sciences, Advanced Medical and Dental Institute, Universiti Sains Malaysia, Pulau Pinang, Malaysia; Dental Simulation and Virtual Learning Research Excellence Consortium, Advanced Medical and Dental Institute, Universiti Sains Malaysia, Bertam, 13200 Kepala Batas, Pulau Pinang, Malaysia.
3. Associate Professor, Department of Dental Sciences, Advanced Medical and Dental Institute, Universiti Sains Malaysia, Pulau Pinang, Malaysia; Dental Simulation and Virtual Learning Research Excellence Consortium, Advanced Medical and Dental Institute, Universiti Sains Malaysia, Bertam, 13200 Kepala Batas, Pulau Pinang, Malaysia.
4. Associate Professor, Department of Dental Sciences, Advanced Medical and Dental Institute, Universiti Sains Malaysia, Pulau Pinang, Malaysia; Research Development Division, Leave a Nest Malaysia Sdn. Bhd., L1-06, Block 3710, Persiaran Apec, Cyber 8, 63000 Cyberjaya, Selangor, Malaysia.
5. Doctor Biomaterials Niche Area Group, School of Material and Mineral Resources Engineering, Engineering Campus, Universiti Sains Malaysia, 14300 Nibong Tebal, Pulau Pinang, Malaysia.

NAME, ADDRESS, E-MAIL ID OF THE CORRESPONDING AUTHOR:
Norehan Mokhtar,
Associate Professor, Department of Dental Sciences, Advanced Medical and Dental Institute, Universiti Sains Malaysia, 13200 Kepala Batas, Pulau Pinang, Malaysia; Dental Simulation and Virtual Learning Research Excellence Consortium, Advanced Medical and Dental Institute, Universiti Sains Malaysia, Bertam, 13200 Kepala Batas, Pulau Pinang, Malaysia.
E-mail: norehanmokhtar@usm.my

PLAGIARISM CHECKING METHODS: [Jain H et al.]
- Plagiarism X-checker: Sep 24, 2024
- Manual Googling: Feb 13, 2025
- iThenticate Software: Feb 15, 2025 (3%)

ETYMOLOGY: Author Origin

EMENDATIONS: 5

AUTHOR DECLARATION:
- Financial or Other Competing Interests: This research was funded by the Fundamental Research Award Scheme (FRGS) grant no. FRGS/1/2018/SKK14/USM/02/7.
- Was Ethics Committee Approval obtained for this study? No
- Was informed consent obtained from the subjects involved in the study? No
- For any images presented appropriate consent has been obtained from the subjects. NA

Date of Submission: **Sep 20, 2024**
Date of Peer Review: **Nov 07, 2024**
Date of Acceptance: **Feb 20, 2025**
Date of Publishing: **Jun 01, 2025**